DRONNINGLUND DISTRICT HEATING MONITORING DATA EVALUATION FOR THE YEARS 2015-2017

Steinbeis Research Institute
for Solar and Sustainable
Thermal Energy Systems
www.solites.de

solites

ON BEHALF OF

PlanEnergi
Jyllandsgade 1
9520 Skørping
Denmark

M.Sc. M.Sc. Carlo Winterscheid

and

Dipl. Ing. Thomas Schmidt

Solites
Steinbeis Research Institute for
Solar and Sustainable Thermal Energy Systems
Meitnerstr. 8, 70563 Stuttgart, Germany
Tel.: +49 711/6732000-0, Fax: +49 711/6732000-99
info@solites.de
www.solites.de

Stuttgart, 30.01.2019

This work is supportet by
EUDP (project no. 64014-0121)

DRONNINGLUND DATA EVALUATION 2015-2017

TABLE OF CONTENTS

1. INTRODUCTION

This report documents the evaluation of the monitoring data for the Dronninglund Fjernvarme solar district heating plant for the years 2014-2017. This work was done within the Danish EUDP project “Follow up on large scale heat storages in Denmark” (project no. 64014-0121). Evaluations for the year 2014 can be found in [Sørensen et.al, 2015].

The report starts with an overview of the overall system heat balance followed by evaluations focused on the renewable parts of the system: solar collector fields, thermal energy storage and heat pump. Minor deviations in heat balances are due to rounding, measurement errors or not measured energy flow streams (e.g. thermal losses of storages).
The pit heat storage, the solar collectors and the absorption heat pump was in operation from March 2014 as part of the project “Sunstore 3”, supported by the national Danish EUDP-program, see [Sørensen et.al, 2015]. The project enables Dronninglund district heating to deliver heating to the consumers from 70 % renewable energy sources where app. 40 % is solar heat. Figure 1 shows the system concept of the plant.

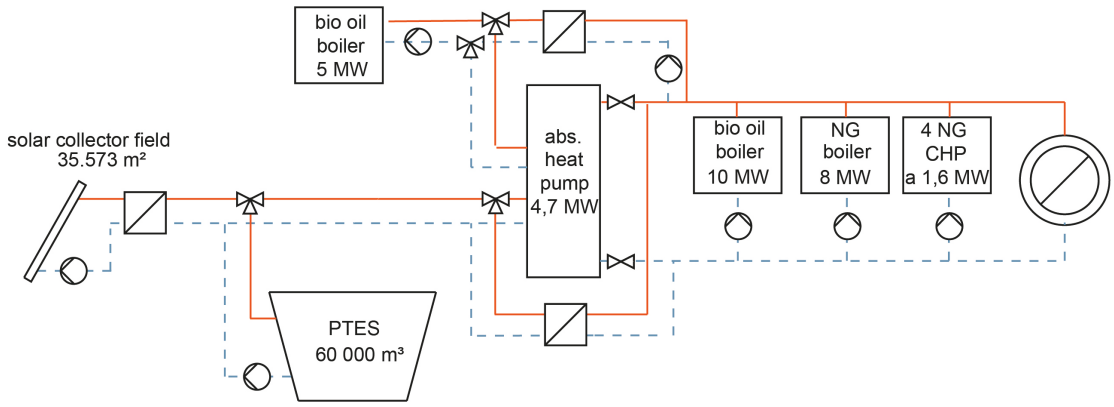

Figure 1: Hydraulic schema of the plant in Dronninglund

2. MONITORING CONCEPT

This section gives a summary of the monitoring concept for the Dronninglund Fjernvarme energy system.

2.1. Monitoring sensors

Figure 2 illustrates the positioning of different sensors in the PTES. At position “A”, water temperature sensors are installed each 0.5 m vertically to qualify the stratification in the PTES. At position “B”, a water level sensor is mounted on top of the diffusor. A heat flux sensor in the middle of the insulation, as well as temperature and humidity sensors above and below the insulation are installed ad position “C”. Finally, position “D” is the location of the rain water pump.

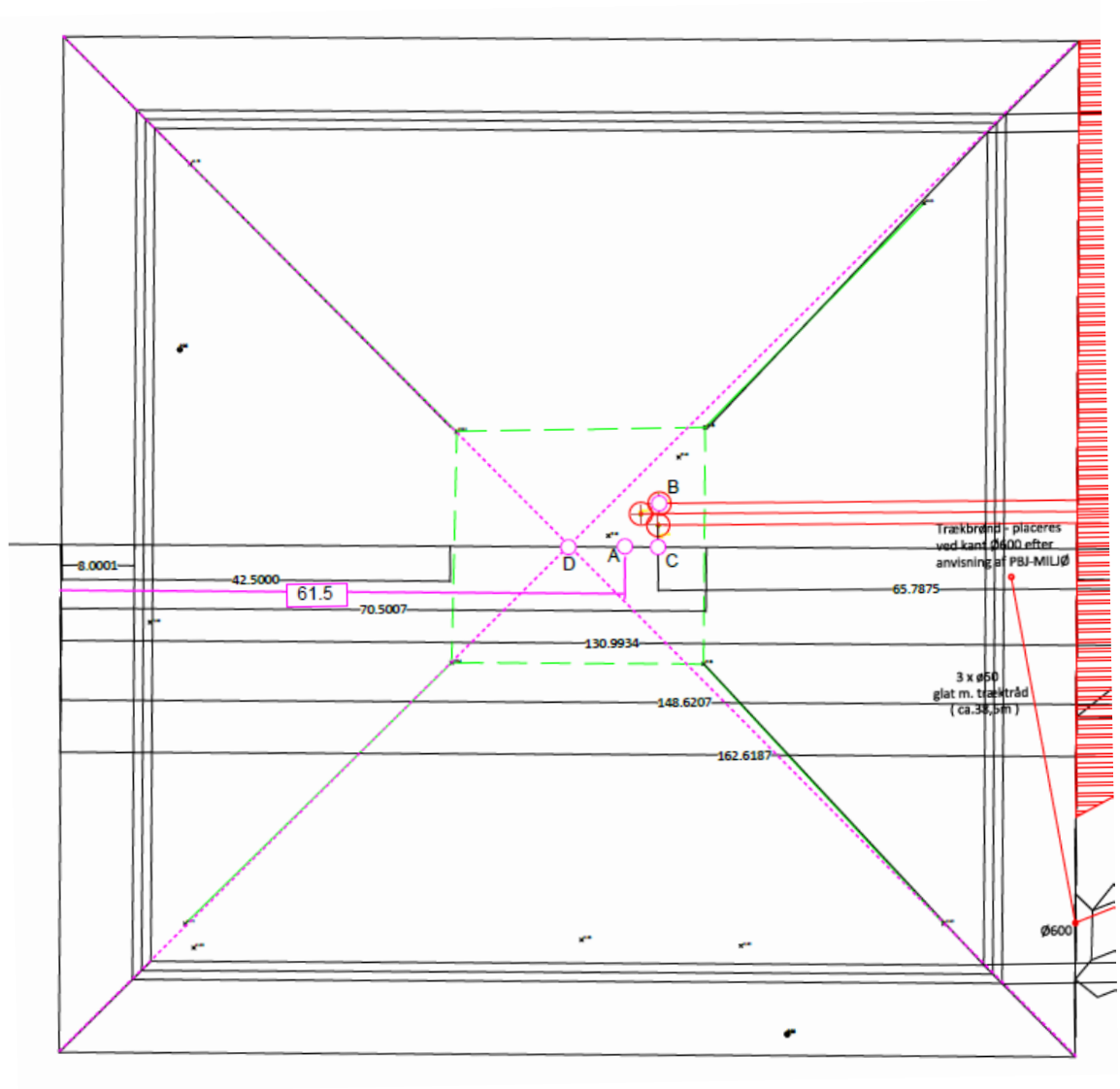

Figure 2: Placement of sensors (source: PlanEnergi)

In addition to the sensors directly in the PTES, four temperature sensors were placed in a depth of 10 m, 15 m, 20 m and 25 m below the water level of the storage on the northern side of the storage. The distance to the storage on water level is between 1 and 2 m. These sensors are used to show the temperature development from the storage to the surrounding soil.

All monitoring sensors are connected to the SCADA[1] system of the plant, all data is stored in a database in 10-minute time steps.

2.2. Evaluation

For the comparison of the efficiencies of different system concepts a number of characteristic numbers, often called key performance indicators (KPI) can be calculated. The ones used in the following sections are:

Solar fraction: $$F_{Sol} = \frac{Q_{Load} - Q_{Aux}}{Q_{Load}} = \left(1 - \frac{Q_{Aux}}{Q_{Load}}\right)$$

Q_{Load}: heat supply to the DH network

Q_{Aux}: auxiliary heat delivered to the system (by boilers, CHP, el. demand heat pump etc.)

Solar collector field efficiency $$\eta_{Coll} = \frac{Q_{Coll}}{G_{sol}}$$

G_{Sol}: global irradiation in solar collector pane

Q_{Coll}: heat delivered by the solar collector field

Storage efficiency $$\eta_{STES} = \frac{Q_{STES,out} + dQ_{STES}}{Q_{STES,in}}$$

$Q_{STES,in}$: heat charged into the seasonal thermal energy storage (STES)

$Q_{STES,out}$: heat discharged from the STES

dQ_{STES}: difference in STES internal energy change in the period

No. of storage cycles $$N_{cyc} = \frac{Q_{STES,out}}{Q_{STES,max}}$$

$Q_{STES,max}$: maximum heat capacity of the STES

[1] SCADA: Supervisory Control and Data Acquisition

3. SYSTEM HEAT BALANCE

Table 1 gives an overview with relevant performance indicators for the years 2015 to 2017 for the solar collector array, the PTES and the heat pump as well as other heat production facilities.

Table 1: Overview of evaluation results for the considered evaluation period in Dronninglund

		2015	2016	2017
solar irradation on collectors	*MWh*	40631	40327	38674
heat from solar collectors	*MWh*	16793	16071	15121
heat charged into PTES	*MWh*	12760	11855	11120
heat discharged from PTES	*MWh*	11983	10716	11315
PTES internal energy change	*MWh*	-497	93	-583
PTES thermal losses	*MWh*	1275	1046	388
absorption heat pump heat delivery	*MWh*	10300	9446	12194
heat pump driving heat demand	*MWh*	5934	5228	9216
heat pump source heat demand	*MWh*	4375	4019	5398
heat from HT*) bio-oil boiler 5 MW	*MWh*	9894	10187	14350
heat from bio-oil boiler 10 MW	*MWh*	2498	1078	209
heat from gas engines 4*1.6 MW_{th}	*MWh*	8011	11456	8160
heat from gas boiler 8 MW				
heat delivery to DH	*MWh*	35447	36994	36869
key performance indicators				
solar collector field efficiency	*%*	41	40	39
PTES storage efficiency	*%*	90	91	96
PTES no. of storage cycles	-	2.2	1.9	2.2
PTES maximum temperature	*°C*	89	87	84
PTES minimum temperature	*°C*	10	12	9
PTES used heat capacity	*MWh*	5500	5200	5202
heat pump COP	-	1.7	1.8	1.6
solar fraction	*%*	41	41	40

*) HT: high-temperature

Figure 3 shows the measured results for the year 2017 in a heat flow diagram. Compared to the first two years, 2017 has had less irradiation and therefore lower gains in solar heat, while the consumption remained rather constant. In 2017 a solar fraction of 40 % was reached, which is slightly below the expected design value of 41 %. The energy from the absorption heat pump, which uses heat from the storage as well as from the high temperature bio oil boiler, increased in 2017.

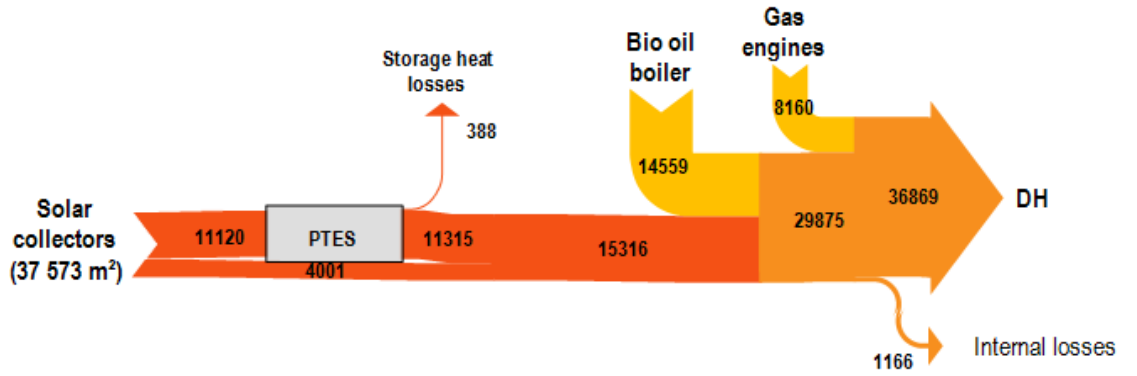

Figure 3: Heat flow diagram according to monitoring data from 2017 (numbers in MWh)

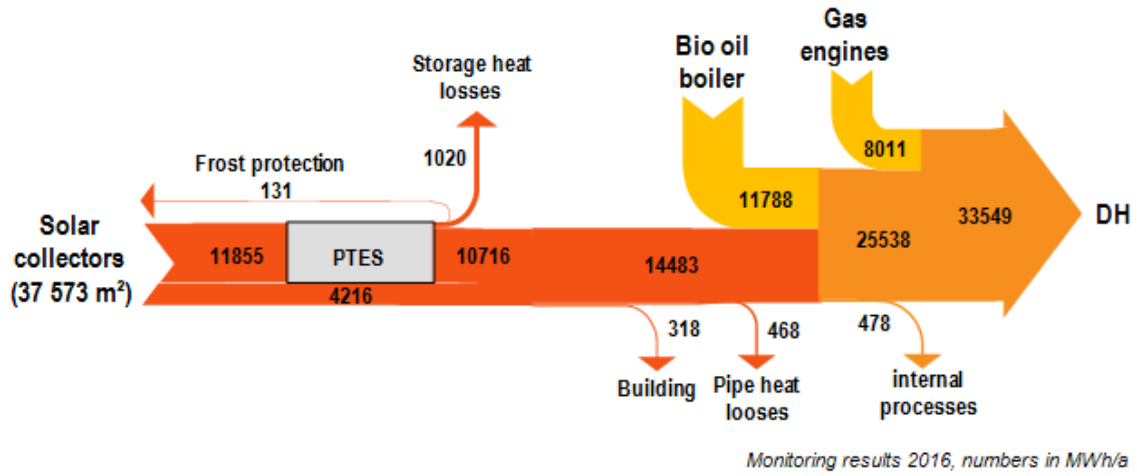

Figure 4: Heat flow diagram according to monitoring data from 2016 (numbers in MWh)

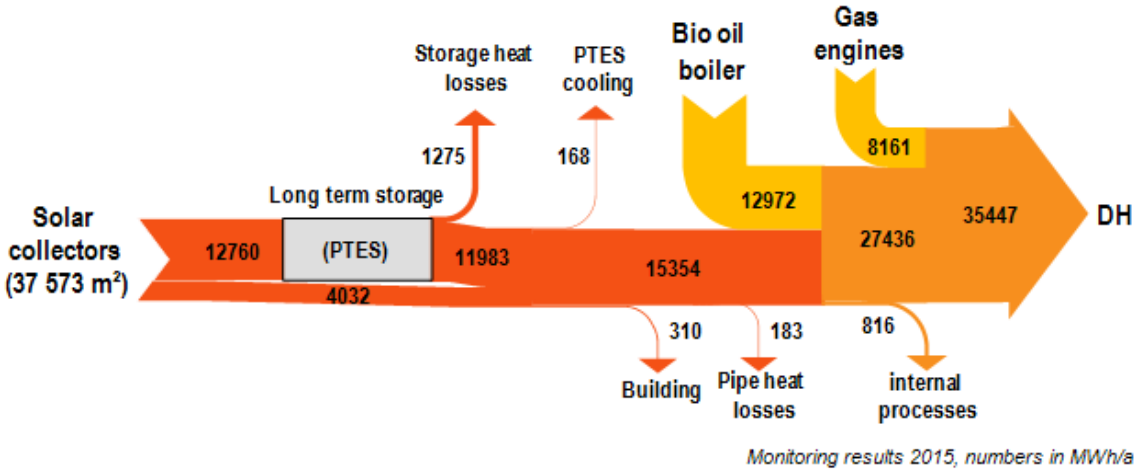

Figure 5: Heat flow diagram according to monitoring data from 2015 (numbers in MWh)

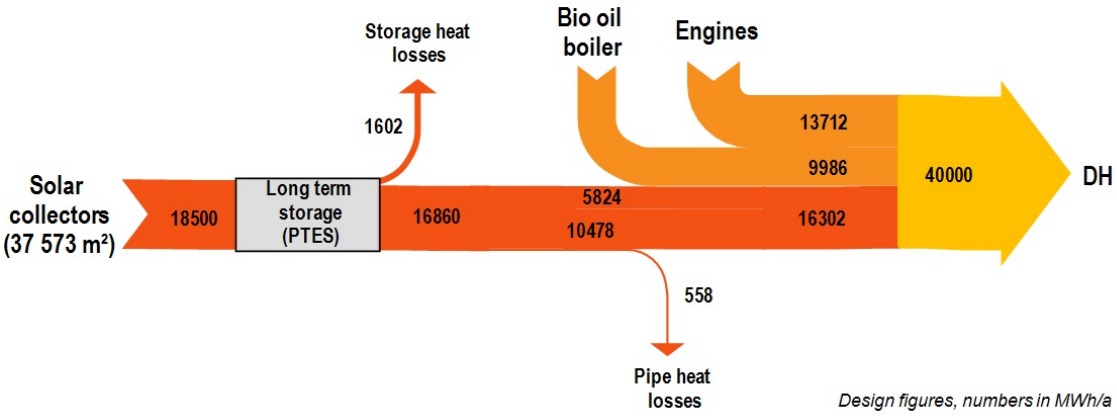

Figure 6: Energy flow diagram of the Dronninglund design figures (numbers in MWh)

Figure 4 and Figure 5 are the corresponding annual heat flow diagrams to Figure 3, for the years 2016 and 2015. Additionally, Figure 6 illustrates the design figures for the plant. One can see that frost protection was only needed in the year 2016 and that the storage heat losses have decrease from 2015 until 2017.
Even though a higher radiation and therefore higher collector yields are measured for 2015 compared to 2016, the solar fraction in the year 2016 was highest compared to the year before. One reason for the higher solar fraction is a lower overall heat consumption in the DH network, as well as reduced heat losses compared to the first year of operation.

The following Figure 7, Figure 8 and Figure 9 show the monthly energy productions and consumptions for 2017 to 2015. The consumption is visualized as thin bars in the centre of each thick bar. The consumption is based on the load of the DH network, the energy that is stored in the PTES and the transmission line losses.
The production (thick bars) are set up from the bio oil boilers, heat from gas engines and gas boilers, discharging from the PTES, heat from the solar collectors and if applicable frost protection for the collector field.

When the three figures are compared one can always see the base curve of the solar heat input, mainly in the summer months. The charging of the PTES is to the largest extend in late spring and summer. Production and consumption are usually lower in the late summer months. A clearly visible change in the application of a production facility can only be seen for the bio oil boiler. The production by this boiler has decreased over the tree years of monitoring.

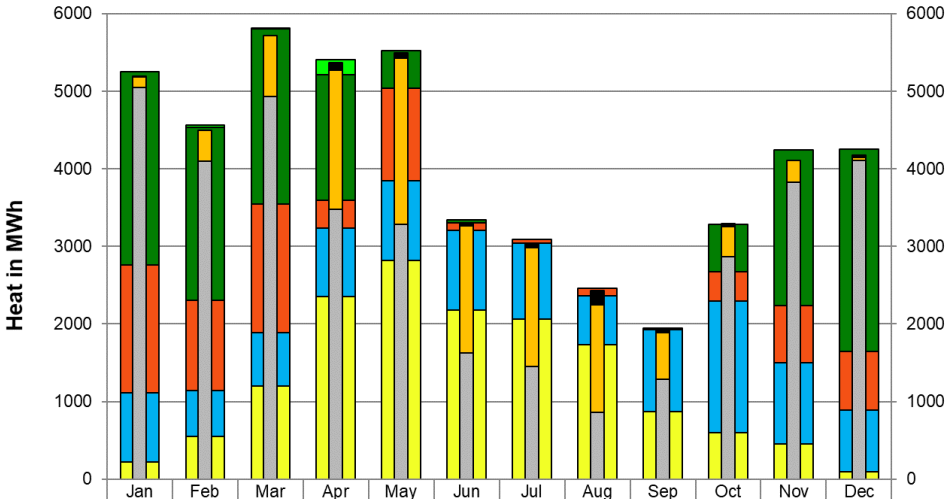

	Jan 2017	Feb 2017	Mar 2017	Apr 2017	May 2017	Jun 2017	Jul 2017	Aug 2017	Sep 2017	Oct 2017	Nov 2017	Dec 2017
bio oil boiler	0	23	0	186	0	0	0	0	0	0	0	0
HT bio oil boiler	2496	2232	2262	1624	478	36	0	0	0	614	2006	2603
heat from gas engines + gas boiler	1647	1162	1656	360	1193	98	48	93	20	379	744	759
discharging PTES	891	593	688	883	1031	1023	978	635	1062	1693	1039	797
solar collectors	220	550	1196	2351	2818	2181	2060	1729	866	601	457	94
frost protection	0	0	0	0	0	0	0	0	0	0	0	0
transmission line losses	4	-15	-26	98	65	34	53	183	31	40	-19	32
charging PTES	135	399	792	1794	2144	1636	1527	1388	599	379	283	44
Total heat to DH	5049	4101	4929	3477	3282	1626	1454	859	1288	2872	3829	4105

Figure 7: Monthly system heat balance for 2017

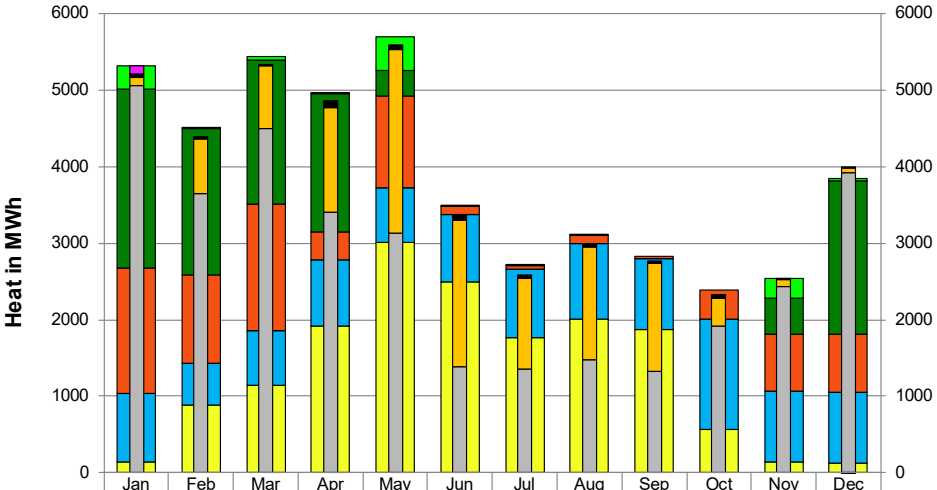

	Jan 2016	Feb 2016	Mar 2016	Apr 2016	May 2016	Jun 2016	Jul 2016	Aug 2016	Sep 2016	Oct 2016	Nov 2016	Dec 2016
bio oil boiler	302	0	40	0	440	0	0	0	0	0	267	28
HT bio oil boiler	2334	1896	1878	1814	328	0	0	0	0	0	456	1995
heat from gas engines + gas boiler	1647	1162	1656	360	1193	98	48	93	20	379	744	759
discharging PTES	881	538	709	870	720	886	890	988	925	1441	937	931
solar collectors	150	892	1146	1911	3004	2488	1768	2011	1878	561	137	127
frost protection	102	29	0	0	0	0	0	0	0	0	0	0
transmission line losses	58	14	28	73	42	77	50	40	35	55	15	-20
charging PTES	94	707	808	1373	2390	1900	1187	1480	1407	362	85	61
Total heat to DH	5062	3646	4498	3397	3137	1390	1353	1472	1324	1916	2436	3918

Figure 8: Monthly system heat balance for 2016

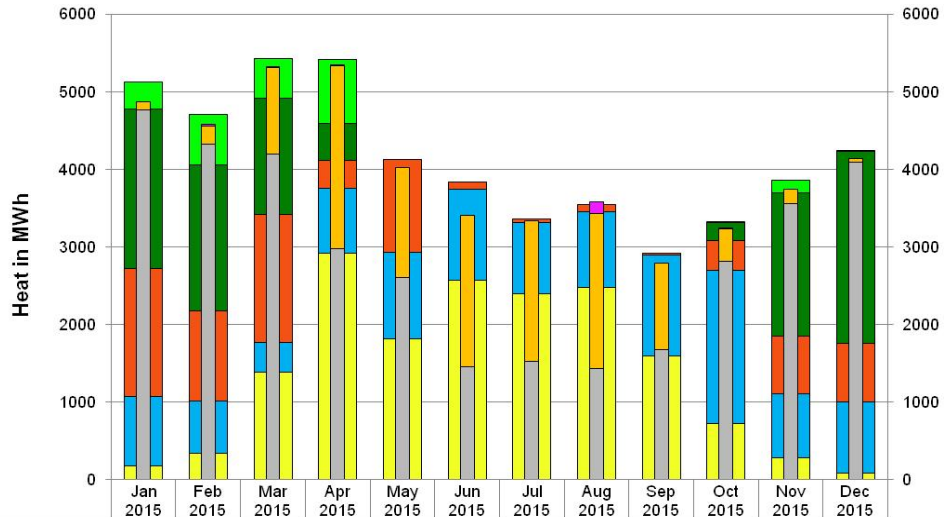

	Jan 2015	Feb 2015	Mar 2015	Apr 2015	May 2015	Jun 2015	Jul 2015	Aug 2015	Sep 2015	Oct 2015	Nov 2015	Dec 2015
bio oil boiler	347	654	511	829	0	0	0	0	0	5	152	0
HT bio oil boiler	2068	1881	1501	473	0	0	0	0	0	230	1847	2474
heat from gas engines + gas boiler	1647	1162	1656	360	1193	98	48	93	20	379	744	759
discharging PTES	897	672	381	833	1117	1167	911	975	1303	1982	827	918
solar collectors	175	347	1386	2923	1820	2576	2403	2477	1594	722	287	83
PTES cooling*)	0	17	0	0	0	0	0	150	0	0	0	0
charging PTES	106	232	1120	2356	1418	1951	1821	1997	1113	423	179	45
Total heat to DH	4768	4332	4199	2977	2607	1456	1524	1431	1680	2814	3564	4096

Figure 9: Monthly system heat balance for 2015

4. SOLAR COLLECTORS

Figure 10 to Figure 12 give an impression of the solar heat production by the solar collector fields in the different years. The production of the two collector fields is stacked on top of each other and the solar irradiation and solar collector field efficiency is shown as connected points. Additionally, the total produced heat and the total area-related produced heat are shown in the top right of the figures.

The solar collector field efficiency is based on the temperatures in and around the solar collector fields. In winter, at times of lower solar irradiation, higher system temperatures and lower ambient temperatures, the efficiency decreases.

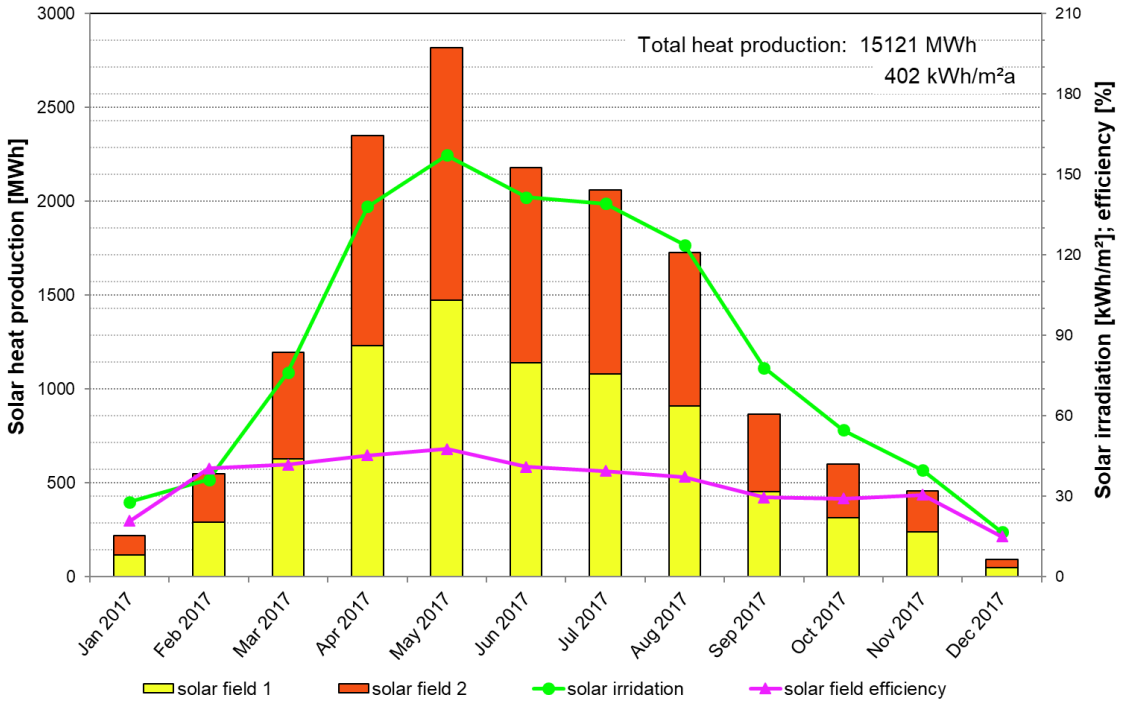

Figure 10: Solar collector heat production in 2017

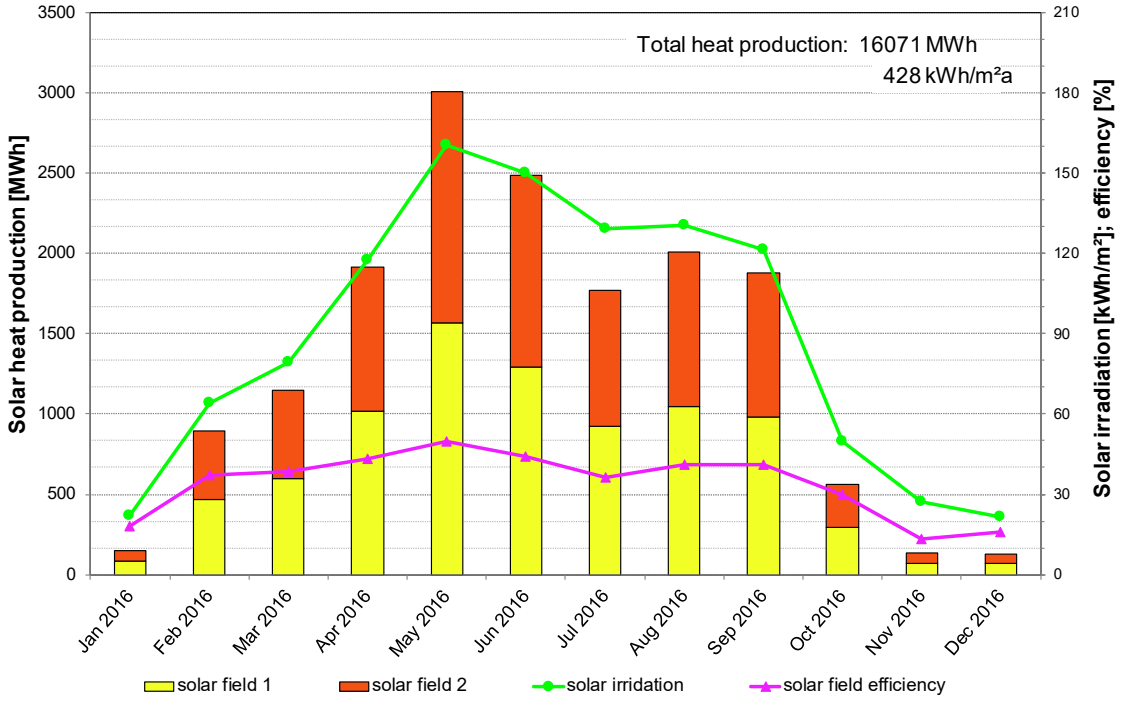

Figure 11: Solar collector heat production in 2016

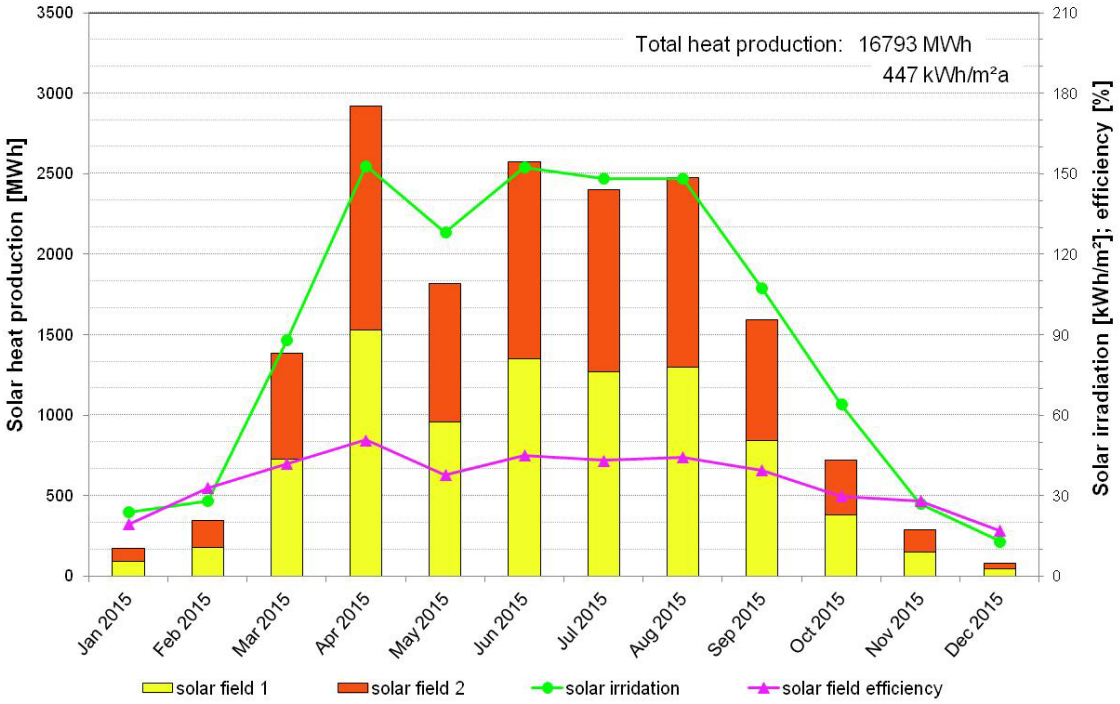

Figure 12: Solar collector heat production in 2015

In Figure 13 to Figure 15, the temperatures on the water side of the heat exchanger of the first collector field can be seen. For the year 2017, one can see that from April to October the solar collectors supplied the temperature required by the DH network. During the other months, lower temperatures were produced. Two different temperature levels can also be observed for the return temperatures. During the winter months, the water from the bottom of the storage is provided to the solar collectors. In summer by contrast, the DH network return temperature level is used.

Figure 16 and Figure 17 show the daily solar gains as a function of the daily solar irradiation. It is visible that the marks for solar field 1 are on average a little bit more left compared to solar field 2. This means, that solar field 1 has slightly higher gains at the same radiation compared to solar field 2.

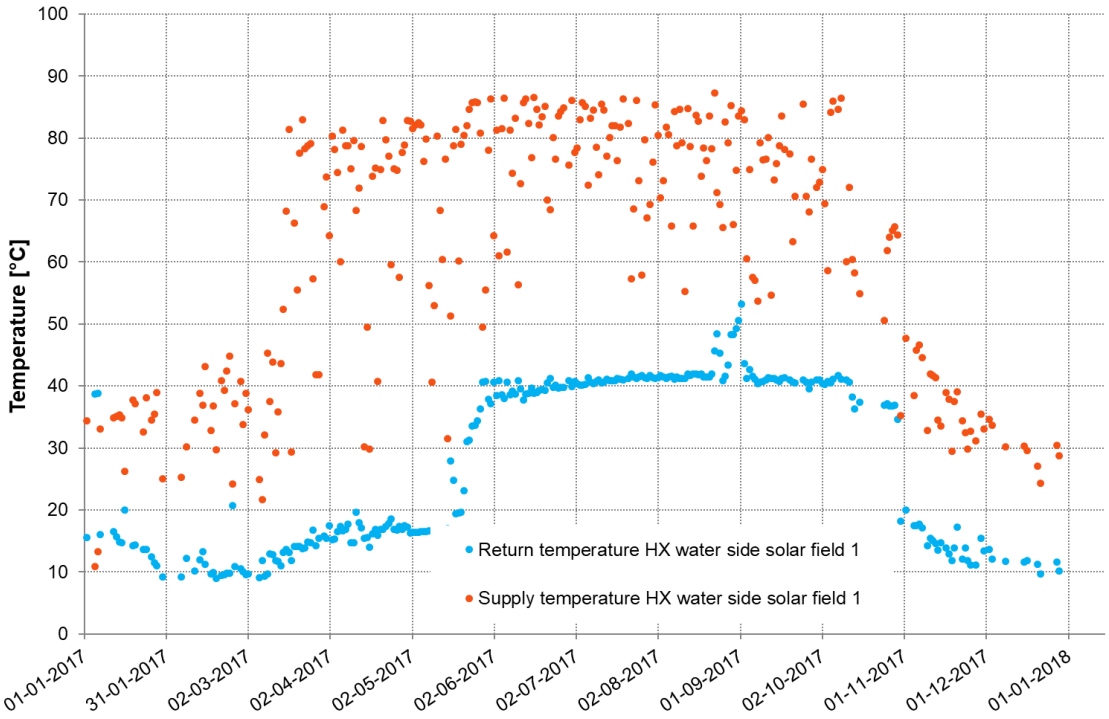

Figure 13: Operating conditions of the solar collector field 1 in 2017 (flow weighted daily mean values at the water side of the solar heat exchanger)

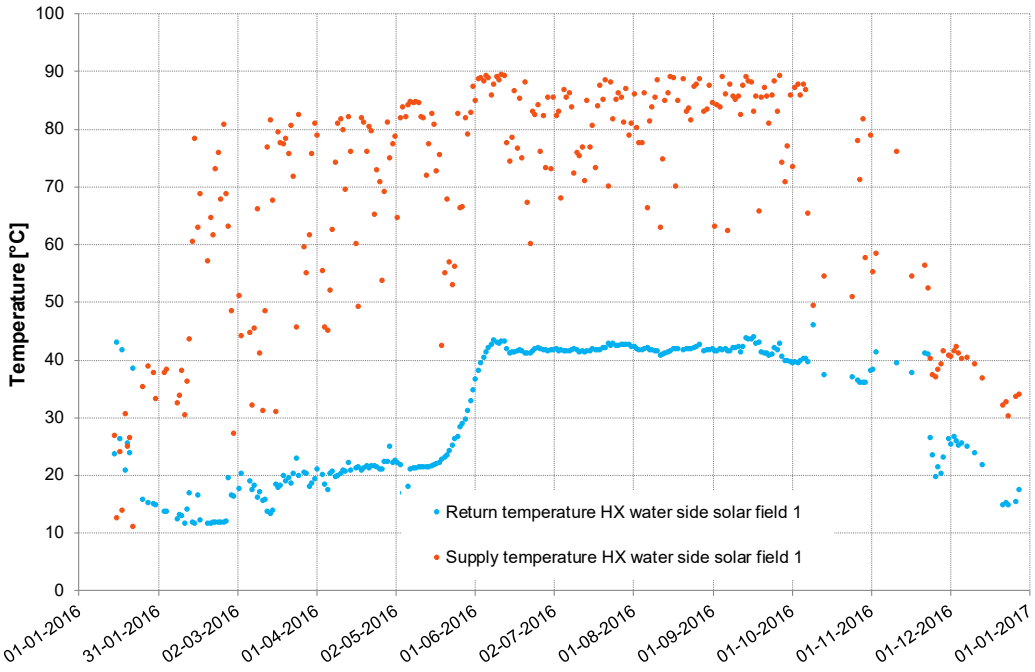

Figure 14: Operating conditions of the solar collector field 1 in 2016 (flow weighted daily mean values at the water side of the solar heat exchanger)

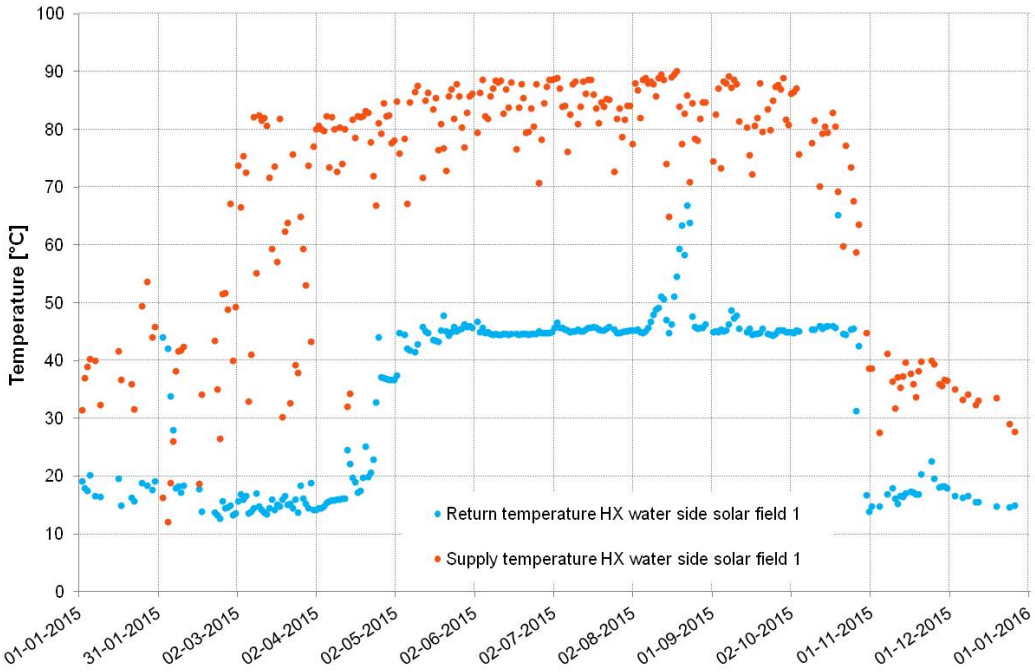

Figure 15: Operating conditions of the solar collector field 1 in 2015 (flow weighted daily mean values at the water side of the solar heat exchanger)

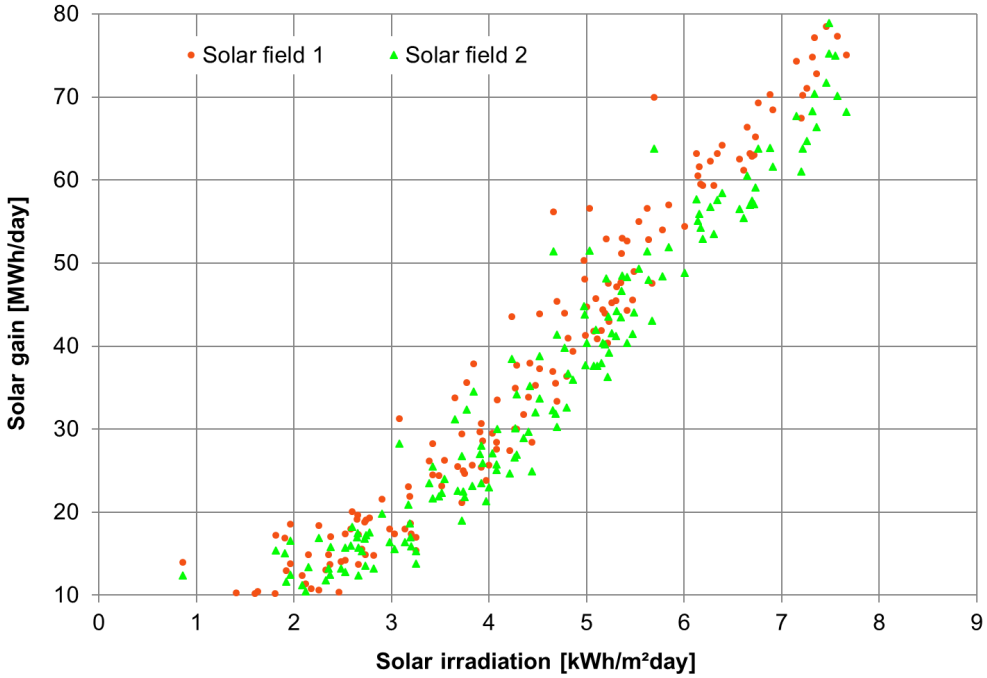

Figure 16: Heat production of the two solar collector fields as a function of the solar irradiation into corresponding solar collector area 2017

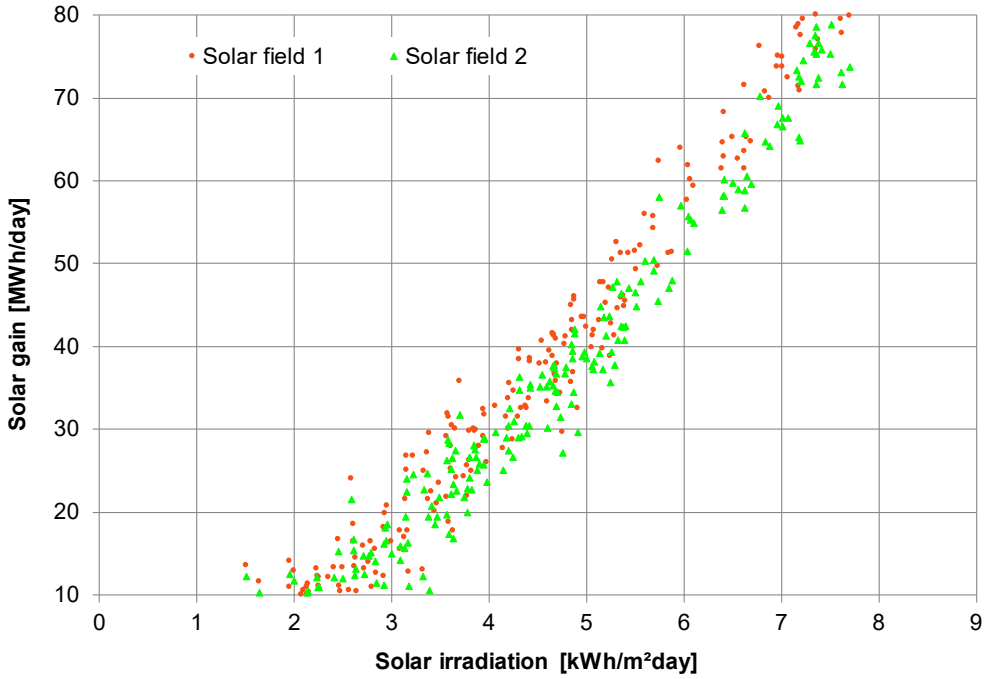

Figure 17: Heat production of the two solar collector fields as a function of the solar irradiation into corresponding solar collector area 2016

5. PIT THERMAL ENERGY STORAGE

The energy balance of the PTES in the year 2016 is presented in Figure 18. Table 1 (column '2017') shows the corresponding key figures that can be calculated from the energy values in Figure 18. The internal energy content of the storage is calculated based on temperature sensors that are installed in the water volume every 0.5 m in vertical direction. The thermal losses can be derived from the energy balance around the PTES.

Figure 21 shows the energy figures for the PTES from 2015 to 2017. The yearly numbers in general show only minor variations, which is an indicator for a rather stable and similar yearly operation of the storage. The only exception are the storage losses, which declined since the beginning. The year 2017 had especially low values for the thermal losses, which can be explained by lower storage temperatures, which also allowed recovering energy from the surrounding soil. Furthermore, a large amount of discharged heat was used by an extensive operation of the heat pump.

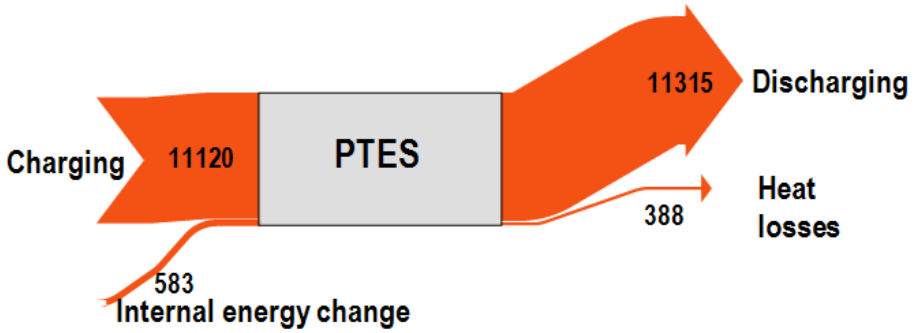

Figure 18: Yearly heat balance for the PIT thermal energy storage for 2017 (numbers in MWh)

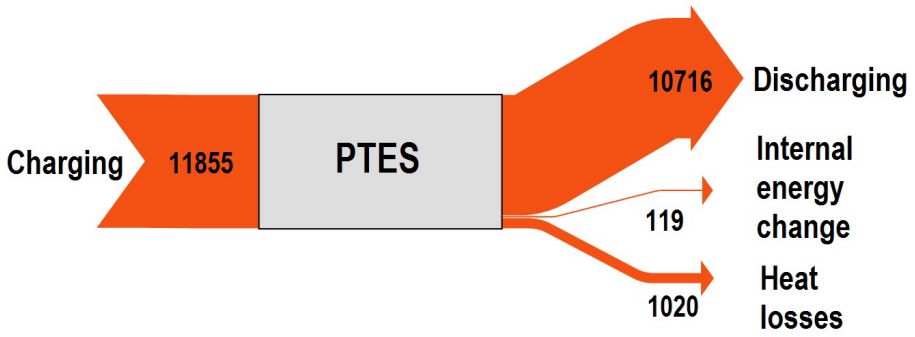

Figure 19: Yearly heat balance for the PIT thermal energy storage for 2016 (numbers in MWh)

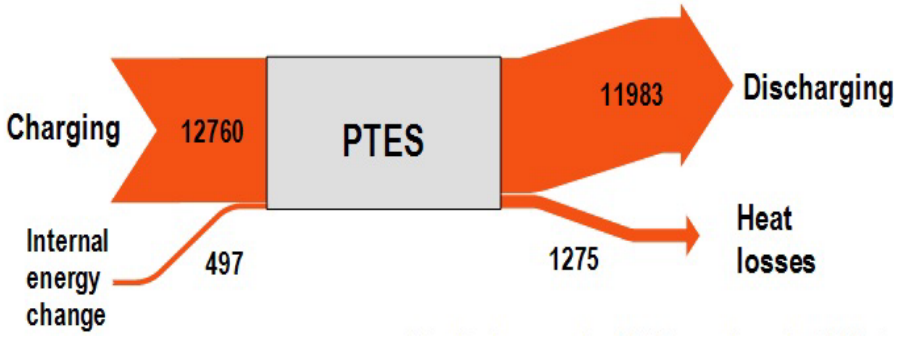

Figure 20: Yearly heat balance for the PIT thermal energy storage for 2015 (numbers in MWh)

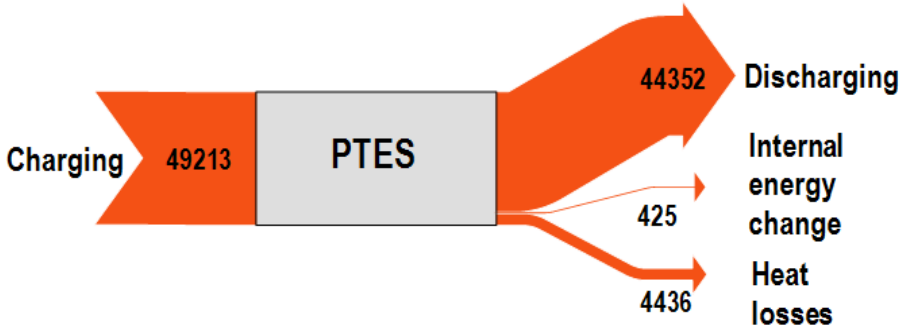

Figure 21: Heat balance for the PIT thermal energy storage for the period 2015 to 2017 (numbers in MWh)

The evaluated mean storage efficiency of around 90 % in 2015 and 2016 is according to design expectations. Compared to the PTES in Marstal the higher efficiency is on the one hand result of lower thermal losses of the PTES in Dronninglund. On the other hand, also the energy turnover of the Dronninglund PTES is twice as much as in Marstal, what is indicated by a mean storage cycle number of 2 instead of only 1 in Marstal. As the thermal losses of the storage are mainly depending on the surface temperatures and not on the energy turnover, a higher energy turnover reduces the effect of the thermal losses on the efficiency number. In addition, the minimum storage temperatures in winter are lower than the surrounding ground temperatures in some parts of the storage, see Figure 26. This means that in these periods there are negative heat losses in the bottom areas.
A storage efficiency of 96 % in 2017 seems unrealistic high. However, when looking into the numbers given in Table 1, one can see that the amount of heat discharged from the storage is higher than the amount of heat charged into the storage in 2017. This is only possible because of the heat pump, that was used more extensively in 2017 compared to the years before. In 2017 the energy used as source heat from the PTES for the heat pump accounted for about 5400 MWh, which is more than 1000 MWh more compared to 2015 and 2016 (see Table 1).As a consequence of this, the temperatures in the storage are lower for longer periods of the year. An analysis of the temperatures in the storage in a depth of 8 m shows, that in 2016 the lower part of the storage had temperatures below 15 °C for about 940 hours, whereas in 2017 the duration was higher than 2200 hours. In these periods the temperatures in the surrounding ground are higher than the temperatures inside the storage. This leads to a heat transfer from the underground into the storage in the lower parts of the storage and thus to negative heat losses. This also explains the low overall thermal losses of the storage in 2017. Negative heat losses cannot be confirmed directly from the monitoring data, as no suitable monitoring sensors for this are available, but have been verified in a recent simulation study that was done for the Dronninglund PTES based on monitoring data for 2015.

Figure 22 shows the monthly heat amounts that were charged into and discharged from the PTES since start of operation in 2014 until 2017. It can be seen that besides the seasonal storage process from summer to winter the storage is also used for short-term storage processes in the summer period. These additional short-term storage processes lead to the larger energy turnover in comparison with the Marstal PTES that was already discussed above in conjunction with the storage cycle number.

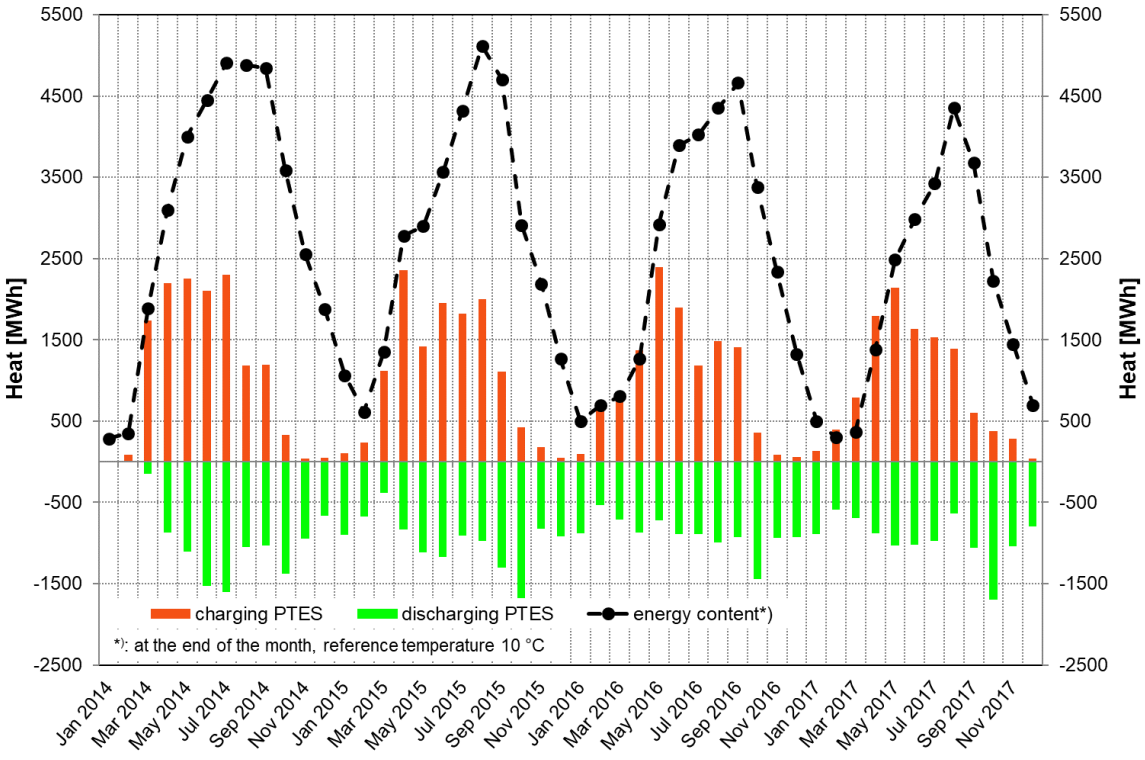

Figure 22: Monthly overview of charging and discharging of the PTES in Dronninglund from 2014 till 2017

5.1. PTES ground temperatures

The temperature development inside the storage volume can be seen in Figure 23 for the year 2017. Similarly, the behaviour of the storage can be observed since start of storage operation in Figure 24. Generally, the maximum temperatures at the top of the storage in summer are a little higher than 85 °C, minimum temperatures go down to 10 – 15 °C at the bottom. The minimum temperature at the top is around 20 °C in winter. Temperature differences between top and bottom reach almost 50 K in spring and 40 K in autumn.

In the discharging periods clear steps can be seen in the bottom temperatures (blue lines) in October / November. During this time the connected heat pump starts operation and allows for a discharging of the storage far below the return temperature level of the DH network.

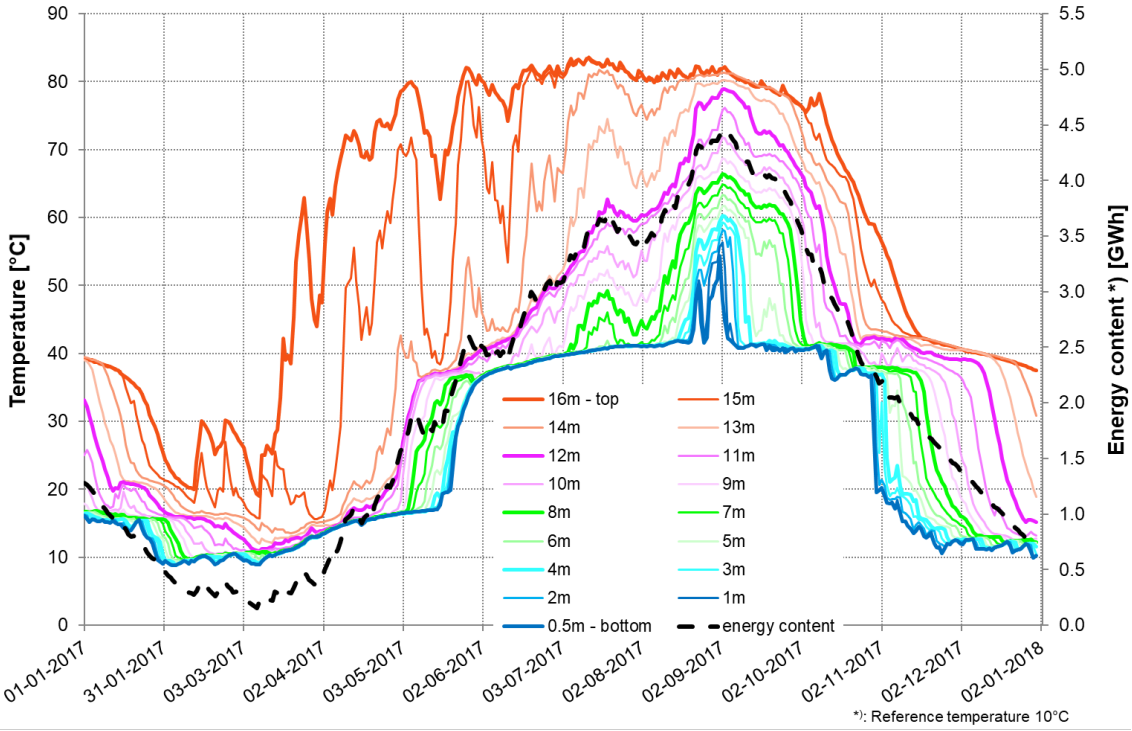

Figure 23: Temperature distribution on the PTES during the year 2017

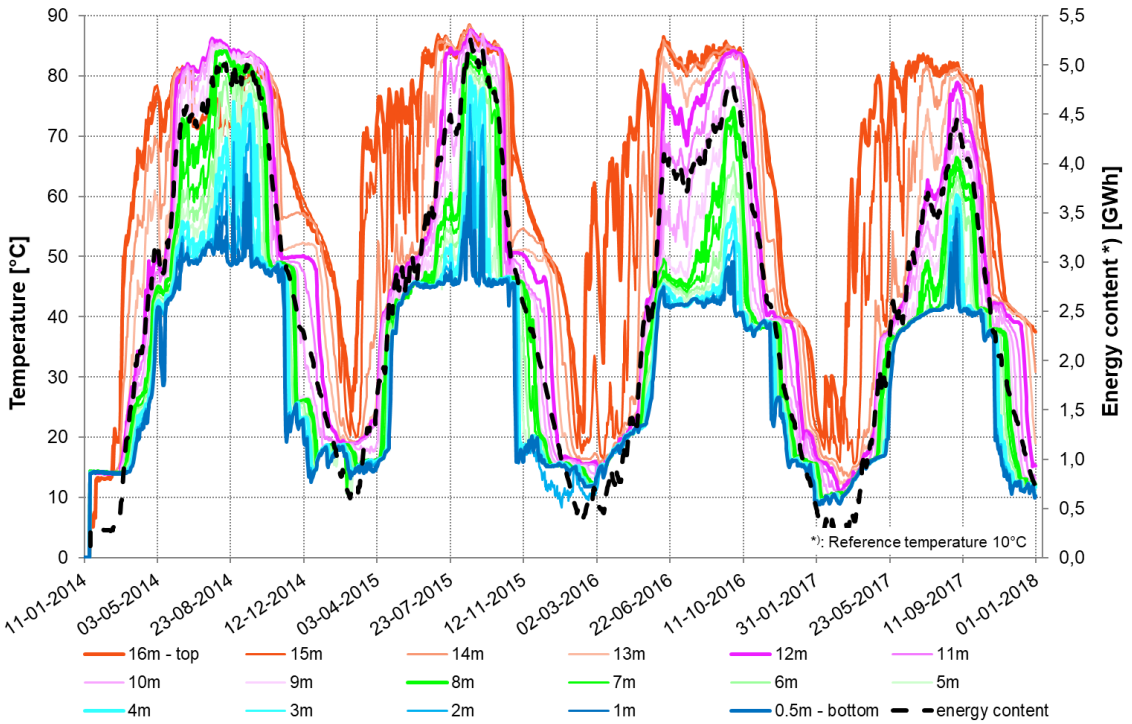

Figure 24: Temperature distribution and energy content in the PTES from 2014 to 2017

Figure 25 shows the ground temperatures depending on the depth for each month in 2017. The temperature can be read out depending on the depth below the water surface, which is shown on the y-axis. From June to September higher temperatures can be seen in the top and bottom of the storage. When comparing these lines one can see that the storage is charged from the top. The top warms up first and deeper layers at a later point. One can also see that the temperatures in the bottom are higher in summer and fall than in spring and winter.

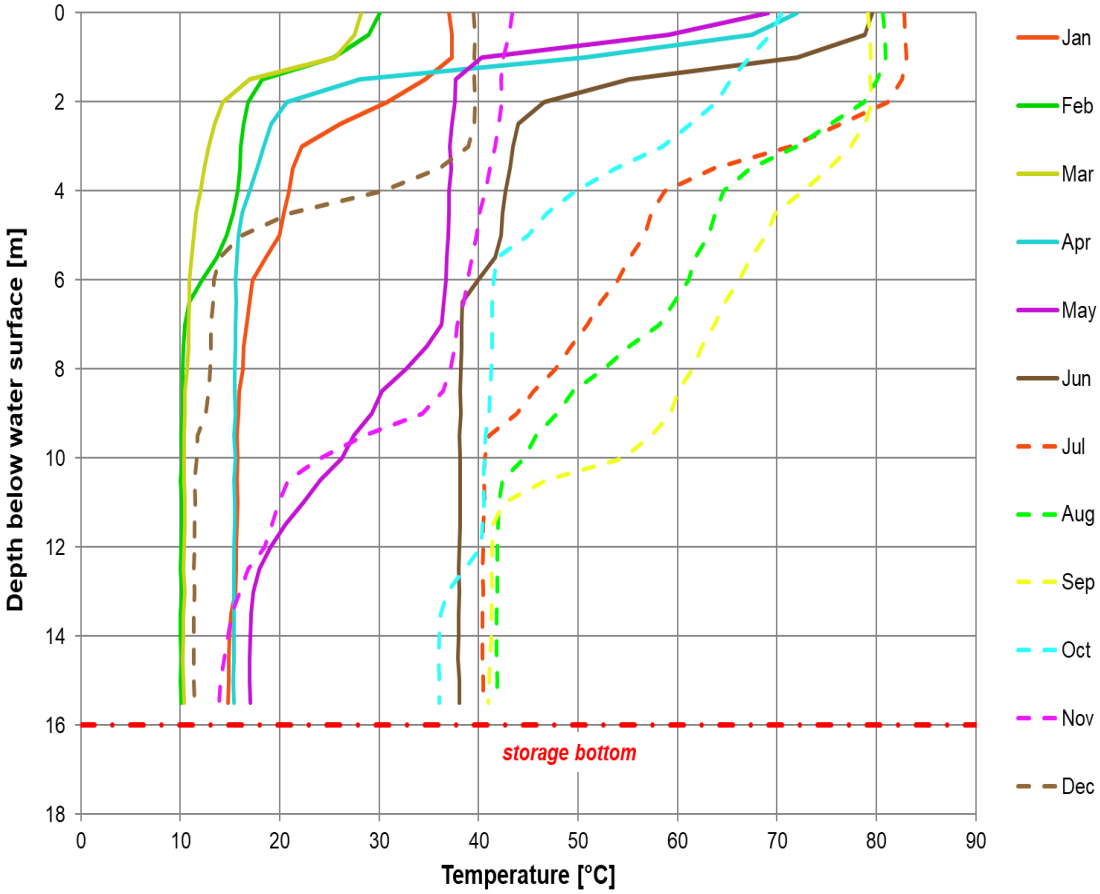

Figure 25: Ground temperature development in 2017 (measured on the 15th day of each month)

Four different sensors at different depths measure the ground temperatures outside the storage. Figure 26 shows a graph with the temperatures since the beginning of the PTES operation. One can see the influence of depth by the variance of the temperatures throughout the seasons. The lower sensors measure rather steady temperatures, which are slowly increasing. Since the beginning of operation, the temperatures in a depth of 20 m and 25 m have risen about 2 to 3 K. The temperatures at 10 m and 15 m depth have increased more than 5 K between the start of measurement and their collapse in 2016 and 2017. Clearly visible in the upper temperature developments are seasonal changes. The annual peak of the sensors in 10 and 15 m depth are delayed by about 3 months.

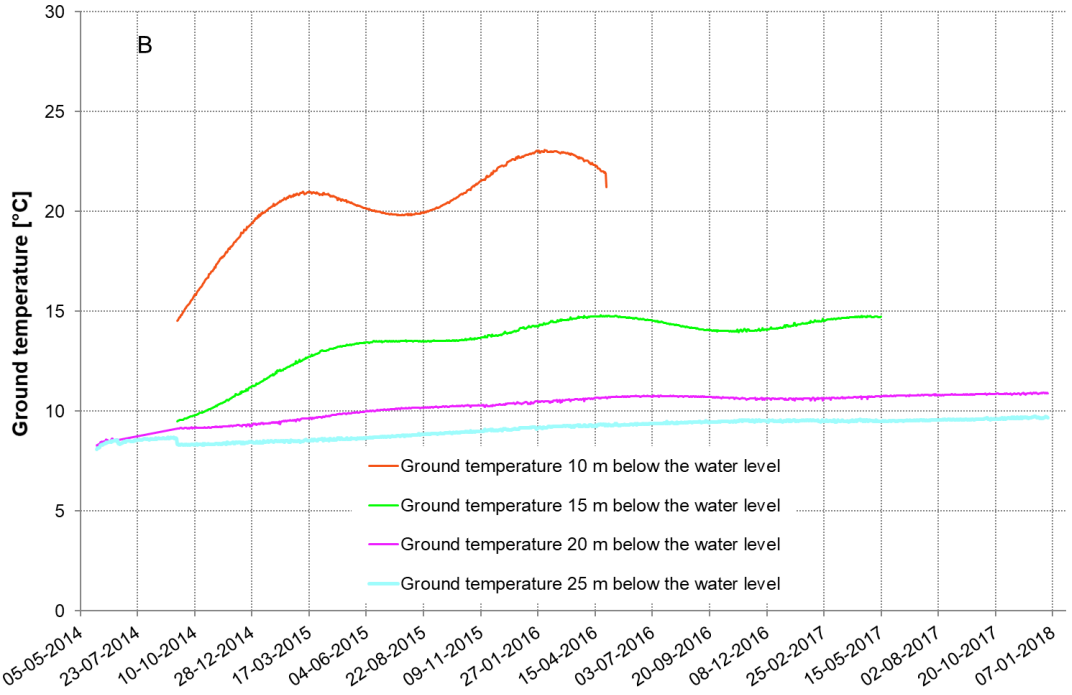

Figure 26: Temperature measurements in the ground in a distance of about 1-2 m to the storage water surface centrally on the northern side of the storage

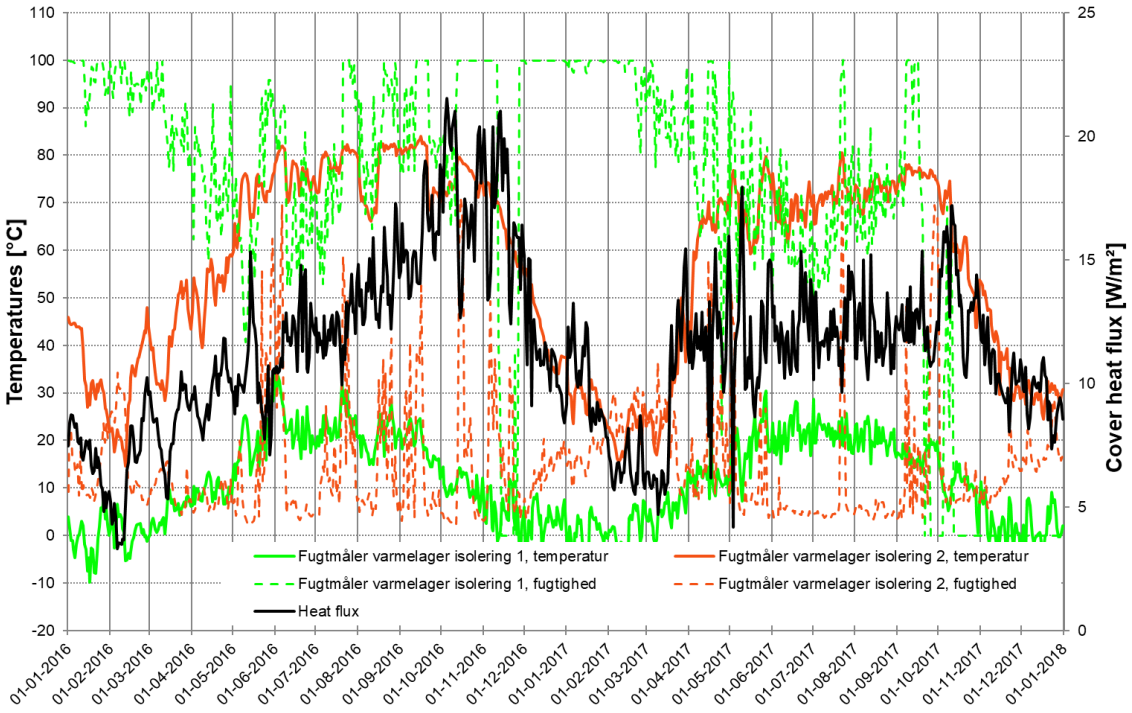

Figure 27: Temperature and heat flux in the storage lid in 2016 and 2017

Figure 27 visualizes measurements from sensors at one position in the PTES lid. For this location the inside and outside temperatures in the insulated floating lid are measured. Additionally, the heat flux and the humidity in the lid insulation are measured. When comparing the year 2016 and 2017, one can see lower maximum temperatures in 2017 and a lower heat flux, especially during autumn time.

6. HEAT PUMP

The following three graphs show the performance of the absorption heat pump for 2015 to 2017. The total heat production found its maximum in 2017 with 14,852 MWh, which is considerable higher than in the previous years where it has been around 10,000 MWh. The heat pump is used to extract heat from the storage, when the temperature is too low for direct use. Therefore, the main operation of the heat pump is in winter and spring.

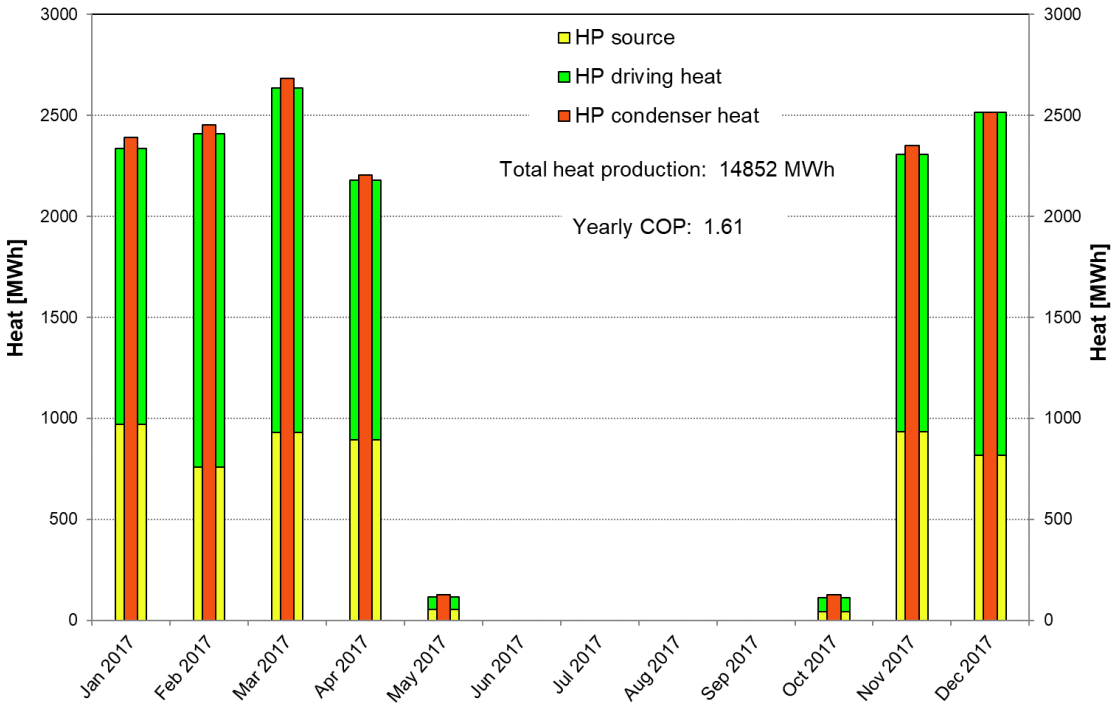

Figure 28: Monthly heat balance of the heat pump in 2017

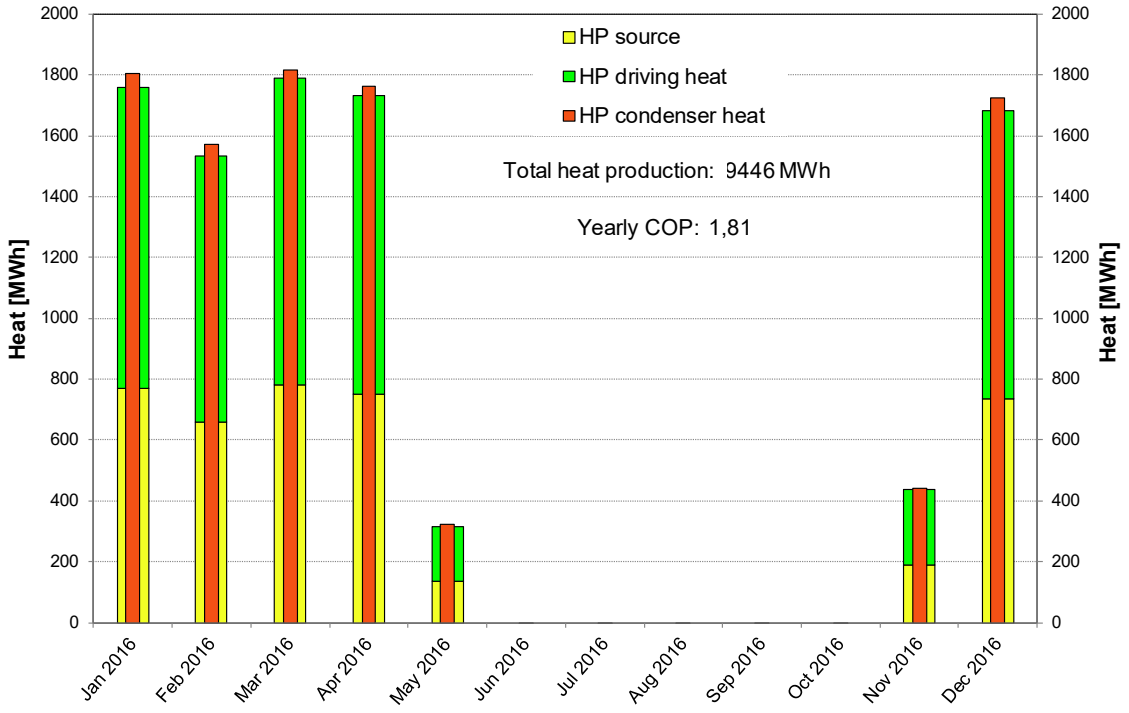

Figure 29: Monthly heat balance of the heat pump in 2016

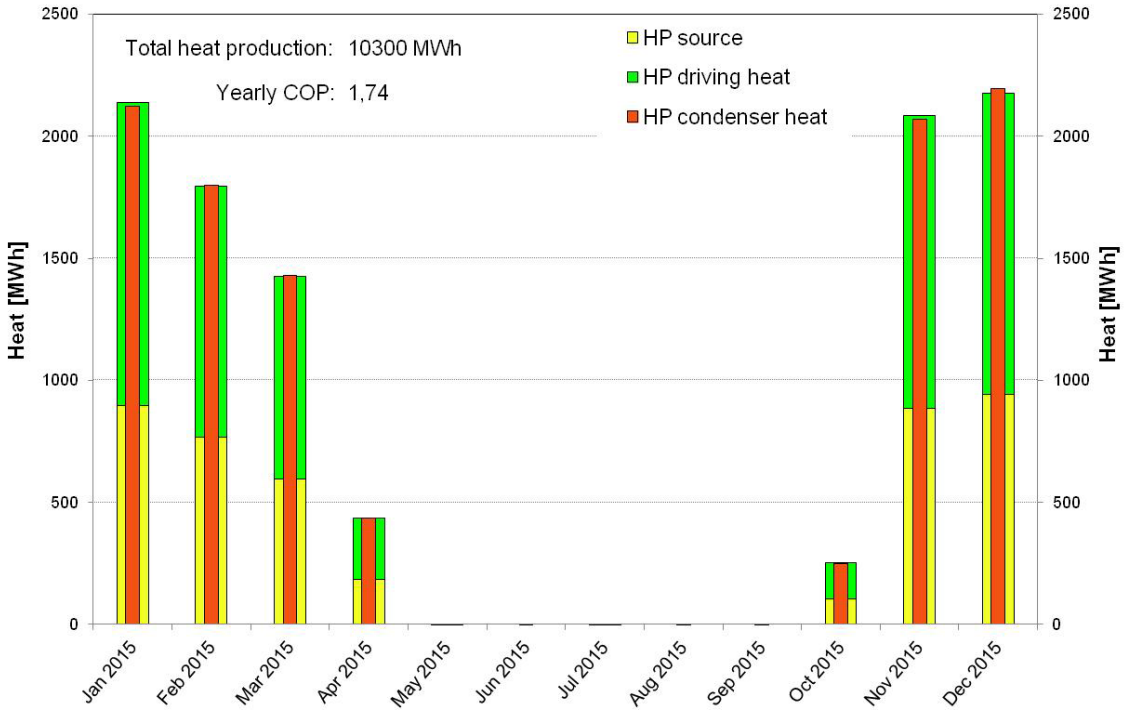

Figure 30: Monthly heat balance of the heat pump in 2015

Figure 31 to Figure 33 show the temperatures and the COPs of the heat pump for the years 2015 to 2017. As the COP is highly influenced by the temperature difference that has to be overcome, a larger temperature lift results in a lower COP. In Figure 31 this is clearly visible in the beginning of 2017. The decrease of the source side temperature of the heat pump, combined with the temperature increase on the condenser side leads to a drop in the COPs.
In all three figures, the summer time without operation can be seen as a gap of operation points. In Figure 31 one can also observe a higher source temperature in April, which is caused by the increase in storage temperatures.

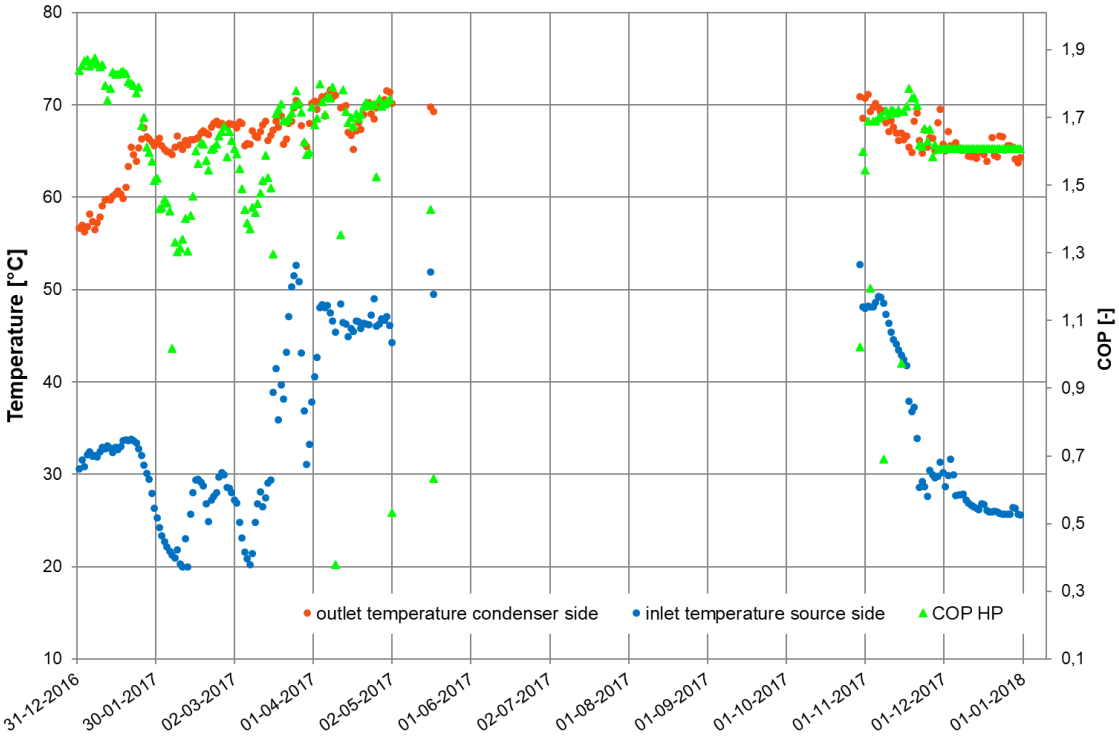

Figure 31: Heat pump operation conditions (weighted daily mean values) of the year 2017

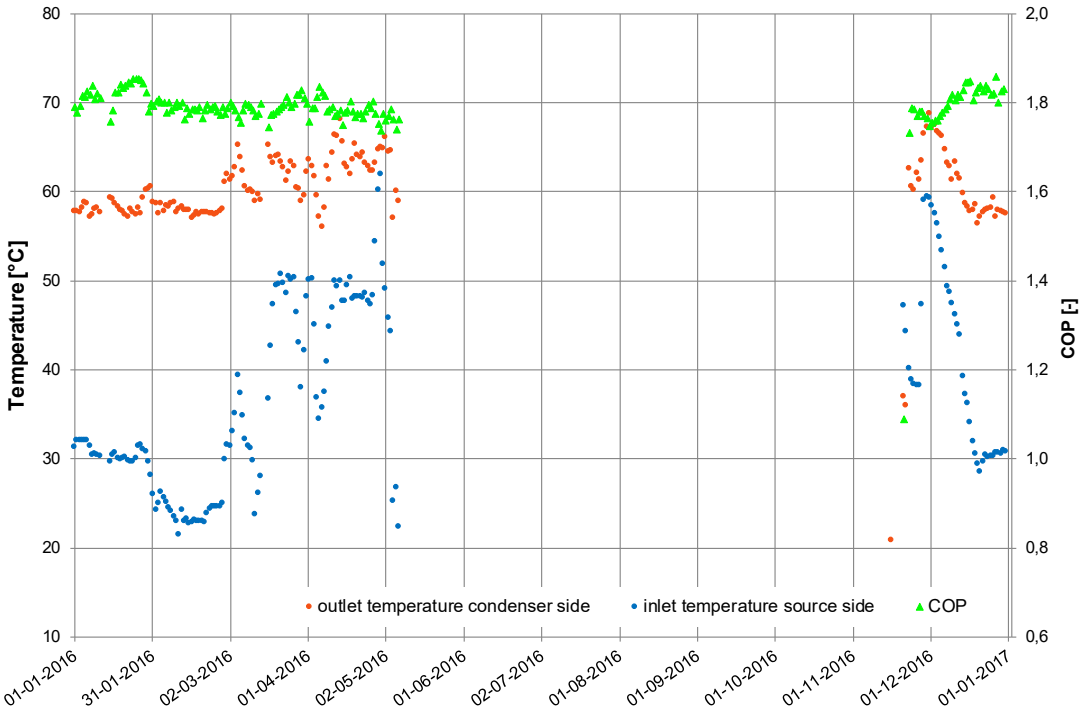

Figure 32: Heat pump operation conditions (weighted daily mean values) of the year 2016

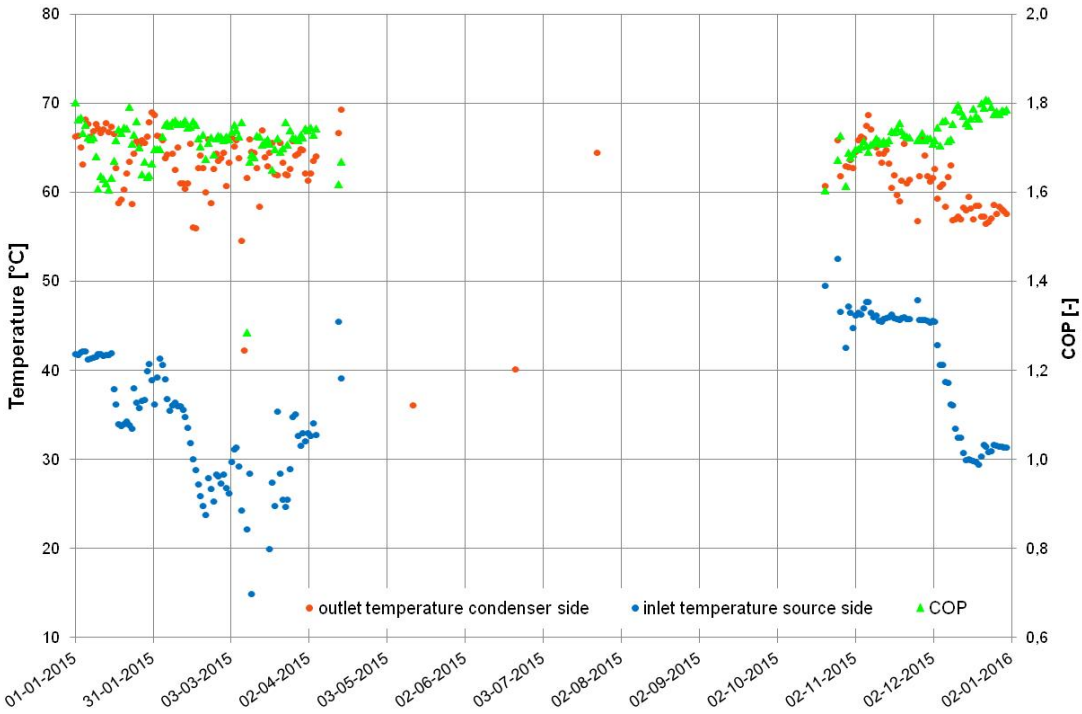

Figure 33:Heat pump operation conditions (weighted daily mean values) of the year 2015

7. SUMMARY

The results from the monitoring data evaluations of the large-scale pit thermal energy storage in Dronninglund prove the efficiency and reliability of the storage technology. The results show good agreements with the design figures in terms of storage efficiency, usable temperature ranges and contribution to the heat supply of the connected district heating networks. Deviations are explainable by different operational conditions or other site specific effects.
The evaluated solar fractions are according to design expectations. The losses of the storage turned out to be lower than expected for all years. One positive impact in this sense are the low temperatures in the storage in the winter period, which result in negative thermal losses in the bottom parts of the storage.

These low temperatures were only possible due to the operation of the heat pump. This allows a nameable increase of the usable temperature differences of the storage and therefore smaller storage volumes are required compared to systems without heat pumps. In Dronninglund the temperatures in the bottom of the storage were about 10 °C, which means it was below the soil temperatures in that region. The highest temperatures decreased from 89 °C in 2015 to 84 °C in 2017. As the majority of heat losses occur at the top of the storage, this reduction has also had a positive impact on the storage losses.

8. REFERENCES

Schmidt & Sørensen 2018 Schmidt, T., Sørensen, P.A.: Monitoring Results from Large Scale Heat storages for District Heating in Denmark, 14th International Conference on Energy Storage, 25-28 April 2018, Adana, Turkey

Sørensen, 2018: Sørensen P.A., “Best practice” for implementation and operation of the Large Scale Borehole and Pit Heat Thermal Storages (BTES and PTES) in Brædstrup, Marstal, Dronninglund and Gram, Denmark, PlanEnergi 2018.

Sørensen et.al., 2015 Sørensen, P.A., Schmidt C., Paaske B.L., Kjæregaard L., Møller Nielsen C., Schmidt, T. : SUNSTORE 3 Phase 2 Implementation, Final report to EUDP projects no. 64009-0043 and 64010-0447, March 2015, Denmark